Desalination and Water Treatment
www.deswater.com

doi: 10.5004/dwt.2019.23906

151 (2019) 295–306
May

Synergistic effect of a magnetic field and carbon nanotubes on the adsorption performance of metal ions and phenols

Lili Jiang[a,*], Zhikai Cui[a], Haitao Yu[b], Xingang Hou[a]

[a]*School of Material Science and Technology, Lanzhou University of Technology, Langongping Road, Lanzhou 730050, Gansu Province, China, Tel./Fax: +86 24 83681545; email: jianglili2002@163.com (L. Jiang); Tel. +86 931 2976378; Fax: +86 931 2976702; emails: cuizhikai@gmail.com (Z. Cui), houxg1958@163.com (X. Hou)*
[b]*Department of Medical Laboratory, The First Hospital of Lanzhou University, No. 1, Donggang Road, Chengguan District, Lanzhou 730000, Gansu Province, China, Tel. +86 0931 8626421; Fax: +86 0931 8619797; email: yuhaitao7707@163.com*

Received 14 May 2018; Accepted 1 February 2019

ABSTRACT

We investigated the synergistic effect of a magnetic field and amino- and sulfhydryl-modified Fe_3O_4/oxidized multi-walled carbon nanotubes (NH_2-SH-Fe_3O_4/o-MWCNTs) on the adsorption performance for Mg^{2+}, Cd^{2+}, and phenol in circulating water. The prepared NH_2-SH-Fe_3O_4/o-MWCNT composites were characterized using transmission electron microscopy, Fourier-transform infrared spectroscopy, hysteresis curves, and X-ray photoelectron spectroscopy (XPS). Moreover, the thermodynamics and magnetic field intensity affecting on the adsorption process were investigated. The influence of magnetic field intensity on the adsorption capacity of the adsorbents was also investigated. The optimal experimental effect was obtained at temperature of 30°C, magnetic field intensity of 0.27 *T*, and flow velocity of 0.17 m/s. The adsorption capacities of the adsorbent for Mg^{2+}, Cd^{2+}, and phenol were 124.27, 19.80, and 40.15 mg/g at 60 min respectively. The adsorption processes for Mg^{2+}, Cd^{2+}, and phenol conformed to pseudo-second-order kinetic model. Additionally, the adsorption processes for Mg^{2+} and Cd^{2+} were consistent with Langmuir isotherm model, while that for phenol was consistent with Freundlich model. The synergistic effect between the magnetic field and NH_2-SH-GO/o-MWCNTs can improve Mg^{2+} and Cd^{2+} adsorption and inhibit phenol adsorption.

Keywords: Carbon nanotubes; Water treatment; Adsorption; Magnetic field

1. Introduction

Circulating water is an indispensable resource in modern steel and iron manufacture. Consumption of industrial water has greatly increased with the rapid development of the steel industry. To save fresh water resources, reduce water consumption, and respond to the policies of Chinese government for energy conservation and emission reduction, steel enterprises have widely applied water-supply modes of circulating cooling water and adopting cooling water after disposing wastewater as make-up water [1]. However, these models lead to several problems, such as pollution of heavy metals and organics in the circulating water. Chemical reagent-based treatment methods can remove heavy metals and organic pollutants from wastewater but cause secondary pollution. Additionally, physical methods, such as radiation and microwave treatments, have not been popularized because the equipment consumes considerable energy. Physicochemical method is emerging and low-cost treatment that provides a preferable affect with minimal secondary pollution. Therefore, it is urgent to develop a non-polluting, low-cost method that provides a steady

* Corresponding author.

1944-3994/1944-3986 © 2019 Desalination Publications. All rights reserved.

treatment affect for removing heavy metals and organics. Sources of heavy metals and organics in wastewater from steel plants mainly include cadmium-containing wastewater from cold rolling plants, lead- and zinc-bearing scrubbing water of blast furnace gas, and wastewater from sintering flue gas containing diverse organics (e.g., benzenes and phenols). When this wastewater flows into natural bodies of water, it threatens the lives of aquatic organisms and impacts human health. Wastewater treatment technologies mainly involve physical, chemical, and biological methods. Many traditional water treatment methods can no longer satisfy the increasing domestic wastewater discharge and water quality standards. In recent years, with the development of magnetic technology, the combination of magnetic fields with water treatment technologies has become a research focus.

Scale prevention and removal was one of the earliest applications of magnetic treatment technologies. In 1945, Vermeriven determined that magnetic water could reduce the production of water scale in boilers. Afterwards, various countries, including the UK and US, successively carried out research on magnetic treatment technologies. However, research in other countries mainly concentrated on the application of permanent magnetic processors. Donaldson and Grimes [2] indicated that a magnetic field could change the structures of scales and change the nucleation and growth rate of calcium carbonate or magnesium carbonate. By focusing on the scale-forming and corrosion problems that frequently occur when employing circulating cooling water, Cang and Zhang [3] examined the quality of static water using a low-frequency gradient electromagnetic field. The scale-inhibition rate reached 35.3% through several circulating water treatments, while the inhibition efficiency improved to 17.5%. Gryta [4] applied a magnetic field in a membrane distillation process and treated seed crystals using the magnetic field in advance. After the magnetic treatment, more calcium carbonate and gaps were present, and the penetration flux decreased. Moreover, the produced precipitations mostly appeared as calcite structures. However, a method combining a magnetic field and adsorption methods has not been reported.

The adsorption method shows an extensive application potential because of its many advantages, such as strong adaptability and removal of multiple pollutants [5]. However, searching for high-efficiency adsorbents is the key to applying the adsorption method. In recent years, the rapid development of nanomaterials (e.g., carbon nanotubes (CNTs)) has provided a possibility to search for high-efficiency adsorption materials. CNTs exhibit unique pore structures and high specific surface areas, and the surfaces of CNTs can load abundant functional groups. Therefore, CNTs show favorable adsorption characteristics [6–10]. Mubarak et al. [11] optimized condition for highest removal of Cd^{2+} at pH 5.0, with dosage 1.0 g, stirring speed and contact time of 100 rpm and 90 min, respectively. The maximum Cd^{2+} adsorption capacities of both FMWCNTs and magnetic biochar were calculated: 83.33 and 62.5 mg/g.

Mahmoud et al. [12] offered the facile synthesis of nanoporous graphene (NPG) and graphene oxide (GO) membranes to open the door for ideal next-generation membranes as cost effective and sustainable alternative for water purification applications. Bandaru et al. [13] realized the loading of –SH groups on the surface of CNTs by coupling cysteamine hydrochloride with purified SWCNTs; the loading of –SH groups greatly improved the adsorption capacity of CNTs for Hg^{2+} (maximum adsorption capacity of 131 mg/g). Zhang et al. [14] realized a high-efficiency treatment for Cu^{2+} by conducting an amination treatment on CNTs. The loading of surface functional groups could effectively improve the adsorption capacity of CNTs. The adsorption capacity of aminated CNTs for Cu^{2+} reached 26 mg/g and sustained 86.6% of its adsorption capacity after five cycles. However, during practical applications, CNTs easily agglomerate and are difficult to separate after adsorption. However, magnetic CNTs can effectively separate materials. The circulating water is treated using the synergistic effect of the magnetic field and the adsorbent, which has not been reported.

The current experiment aims to investigate the influence of combining the magnetic field and CNTs on the adsorption performance of the adsorbents for Mg^{2+}, Cd^{2+}, and phenol. Amino- and sulfhydryl-modified Fe_3O_4/oxidized MWCNTs (NH_2-SH-Fe_3O_4/o-MWCNTs) were synthesized and the adsorbents were characterized using transmission electron microscopy (TEM), Fourier-transform infrared (FT-IR) spectroscopy, hysteresis curves, and X-ray photoelectron spectroscopy (XPS). The circulating water was affected by the synergistic effect between the magnetic field and adsorbents, and the adsorption capacity of the adsorbent for Mg^{2+}, Cd^{2+}, and phenol was investigated. The optimal conditions and factors that influenced the adsorption capacity were determined by applying the orthogonal experiment. The adsorption process was fit using thermodynamic models and magnetic field intensities influencing on adsorption capacity were investigated.

2. Experimental methods

2.1 Materials and reagents

CNTs (pipe diameter: 10–20 nm; length: 5–15 μm; specific surface area: 100–160 m^2/g; purity: > 97%) were purchased from Shenzhen Nanotech Port Co., Ltd. (China). Concentrated sulfuric acid, concentrated nitric acid, ammonia, and acetone were purchased from Tianjin Baishi Chemical Industry Co., Ltd. (China). $MgCl_2{\cdot}6H_2O$, $Cd(NO_3)_2{\cdot}5H_2O$, phenol, $FeSO_4{\cdot}7H_2O$, $FeCl_3{\cdot}6H_2O$, and hydrazine hydrate were purchased from Tianjin Beichen Fangzheng Chemical Reagent Factory (China). 3-Mercaptopropyltrimethoxysilane (MPTS) was purchased from Beijing Lab-bio Company (China).

2.2. Characterization techniques

TEM (JSM-6700F, JEOL) was used to analyze the surface morphology of the composite materials, while FT-IR (Nicolet 5700, Thermo Fisher Scientific) and XPS (ESCALAB 250Xi, Thermo Fisher Scientific) were employed to analyze the components of the samples. A flame atomic absorption spectrophotometer (Z-5000, Hitachi) was used to detect the concentrations of Mg^{2+} and Cd^{2+}, while the concentration of phenol was measured using an ultraviolet-visible spectrophotometer (type DSH-760CRT). The experimental procedure is displayed in Fig. 1. A magnetic adjustable

processor with a range of 0–0.8 *T* was purchased from Shenzhen Yitian Magnetic Materials Co., Ltd. and calibrated using an HT-100 digital teslameter (Model 905, Honor top). Ultrapure water was used for all experiments and prepared using a water purification instrument (UPD-I-20T).

2.3. Preparation of NH_2-SH-Fe_3O_4/o-MWCNTs

The NH_2-SH-Fe_3O_4/o-MWCNT composite was prepared based on known procedures [15,16]. First, CNTs were purified and 2 g CNTs was added to a three-necked bottle with 50 mL of concentrated sulfuric acid (98 wt%). After ultrasonic dispersion for 10 min, 20 mL of concentrated sulfuric acid (65 wt%) was added to the mixture. After ultrasonic dispersion for 10 min, the mixed solution was mechanically stirred for 2.5 h, filtered, and washed with deionized water until its pH was 7. Final, the mixture was placed in a dry oven at 80°C for 12 h to acquire purified o-MWCNTs. Deionized water (20 mL) was added to 40 mg of the purified MWCNTs in which $FeCl_3 \cdot 6H_2O$ (0.582 g), $FeSO_4 \cdot 7H_2O$ (0.300 g), and polyethylene glycol (2 mL) were separately added; the mixture was mechanically stirred for 5 h at 60°C. Next, diluted ammonium hydroxide (2.5 wt%) was slowly added to the solution until the pH of the solution was 9–10. The solution was constantly stirred for 30 min. Then, the temperature was increased to 80°C and sustained for 30 min. The Fe_3O_4/o-MWCNT composite materials were separated using a commercial magnet, washed several times with ethyl alcohol, and dried at 60°C for 12 h. To further modify the groups on the surface of the Fe_3O_4/o-MWCNTs, 50 mg of Fe_3O_4/o-MWCNTs was added into a three-necked bottle with 40 mL of absolute ethyl alcohol. Acetic acid (0.2 mL) was added to the three-necked bottle and 30 μL of MPTS was added dropwise under nitrogen with mechanical stirring. After stirring for 24 h, 25 mL of acetone was slowly added to the solution. The above mixture was added to a three-necked flask with 40 mL of absolute ethyl alcohol and stirred for 5 h. The mixture underwent ultrasonic dispersion for 10 min. Subsequently, with slow mechanical stirring, 0.5 mL of hydrazine hydrate was added and kept for 3 h. The above products were placed in a vacuum drying oven at 80°C for 12 h after being separated. In this way, NH_2-SH-Fe_3O_4/o-MWCNTs were obtained; the specific preparation process is shown in Fig. 2.

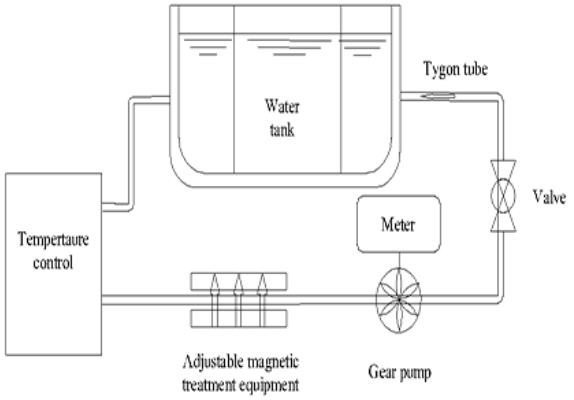

Fig. 1. Devices used to investigate the synergistic effect between the magnetic field and NH_2-SH-Fe_3O_4/o-MWCNTs.

2.4. Synergistic experiment for magnetic field and adsorbent

The orthogonal experiment table $L_9(3^4)$ was initially determined according to the selected influencing factors for the adsorption capacity. According to the orthogonal experimental table, the magnetic field intensity, water velocity, and temperature were adjusted; the influencing factors are shown in Table 1. Ultrapure water (10 L) was added into the circulating water system containing NH_2-SH-Fe_3O_4/o-MWCNTs with a concentration of 50 mg/L. Next, Mg^{2+}, Cd^{2+}, and phenols at an initial concentration of 50 mg/L were added to the circulating water. The adsorption experiment was carried out by turning on the circulating water system to take water samples separately at 5, 10, 15, 30, 60, 90, 120, 180, 240, 300, 360, 420, and 480 min. The concentrations of Mg^{2+}, Cd^{2+}, and phenol in the circulating water were analyzed using an atomic absorption spectrophotometer and UV-visible spectrophotometer. The adsorption capacity of the adsorbents could be calculated using Eq. (1) [10]:

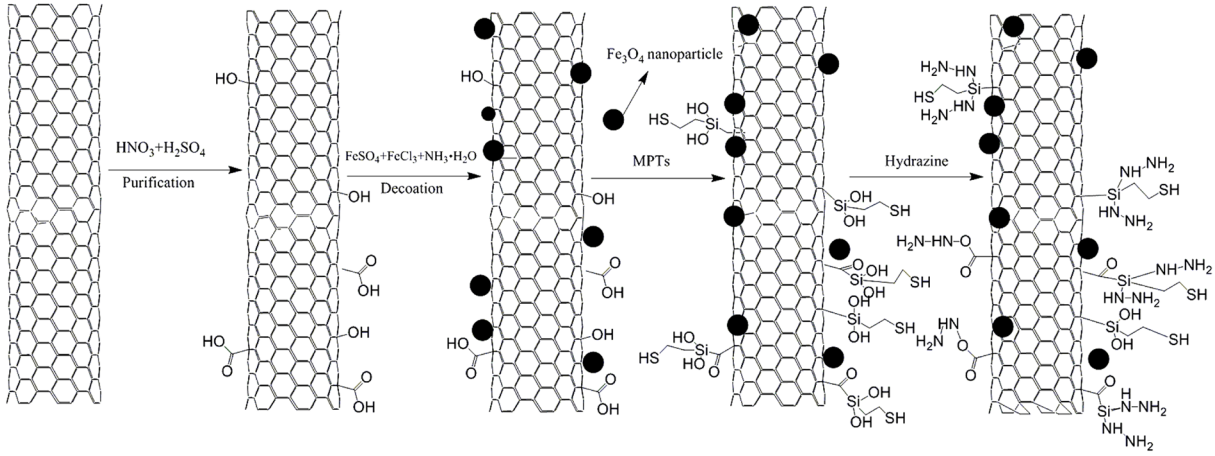

Fig. 2. Preparation process for the NH_2-SH-Fe_3O_4/o-MWCNTs.

$$q_e = \frac{(C_0 - C_e)V}{m} \quad (1)$$

where q_e, C_0, C_e, V, and m refer to the adsorption capacity (mg/g) of the adsorbents at an equilibrium state, initial concentration (mg/L) of adsorbate, concentration (mg/L) of adsorbate at an equilibrium state, volume (L) of the solution, and mass (g) of the adsorbents, respectively. The adsorption data were considered when analyzing thermodynamics and adsorption capacities of adsorbents.

3. Results and discussion

3.1. Results of the orthogonal test

Table 2 shows the results of the orthogonal experiment of circulating water under the synergistic effect between the magnetic field and the NH_2-SH-Fe_3O_4/o-MWCNTs. One of the four selected influencing factors is a blank, and each influencing factor shows three levels. The weight of the adsorption capacities of the NH_2-SH-Fe_3O_4/o-MWCNTs for Mg^{2+}, Cd^{2+}, and phenol were 0.2, 0.4, and 0.4, respectively. The comprehensive score of the sample was calculated using the sum of the multiples between the value of each index and its corresponding weight to divide by the sum of the maximum weights of the indexes in each group. The comprehensive evaluation showed that experiment 5 exhibited the optimal conditions. Namely, the highest adsorption capacity was observed for Mg^{2+}, Cd^{2+}, and phenols under a magnetic field intensity of 0.27 *T* and water velocity of 0.17 m/s at 30°C. Therefore, these conditions were applied for all subsequent experiments. By comparing the values of range *R*, the influencing factor decreased with respect to the temperature, magnetic field intensity, and water velocity. The temperature is the optimal factor that influences the adsorption capacity while the water velocity exhibits the lowest influence on the adsorption capacity.

Table 1
Factors and levels of L_9 (3^4)

Level	Magnetic field intensity (*T*)	Blank column	Temperature (°C)	Velocity (m/s)
1	0	0	18	0.17
2	0.27	0	25	0.34
3	0.54	0	30	0.51

3.2. TEM

Fig. 3 shows TEM images of the original MWCNTs, purified MWCNTs, and NH_2-SH-Fe_3O_4/o-MWCNTs. The TEM image of the original MWCNTs shows that the original MWCNTs had a tubular structure with a diameter of 20–30 nm (Fig. 3(a)). The mutually involved MWCNTs agglomerated and their surfaces exhibited numerous residual impurities from the catalysts; therefore it was necessary to implement the purification treatment. Fig. 3(b) indicates that the diameter of the CNTs that underwent the purification treatment was 30–40 nm. The ends of the MWCNTs were open, which shortened the lengths and improved the agglomeration phenomenon of the MWCNTs. Fig. 3(c) shows that the Fe_3O_4 nanoparticles were uniformly loaded on the surface of the CNTs, with a diameter about 6 nm. The diameter of the NH_2-SH-Fe_3O_4/o-MWCNTs (50–60 nm) was much larger than that of the purified MWCNTs. Numerous Fe_3O_4 nanoparticles were loaded on the surfaces of the CNTs. Fig. 3(d) reveals the energy spectrum of the NH_2-SH-Fe_3O_4/o-MWCNTs. The NH_2-SH-Fe_3O_4/o-MWCNTs contain C, O, N, Fe, Si, and S elements, while the Cu element is taken from the detected base. The C element was derived from the CNTs, while the O element appeared because of the presence of numerous oxygen-containing groups (carboxyl and hydroxyl) on the surface of the CNTs. The existence of the N element implied that amino groups were loaded on the

Table 2
Results of L_9 (3^4)

	Magnetic field intensity (*T*)	Blank column	Temperature (°C)	Velocity (m/s)	Adsorption capacity (mg/g)			
					Mg^{2+}	Cd^{2+}	Phenol	Comprehensive evaluation
1	0	1	18	0.17	107.45	18.92	46.52	0.8535
2	0	2	25	0.34	115.45	18.73	47.31	0.8693
3	0	3	30	0.51	124.91	19.58	48.72	0.9093
4	0.27	1	25	0.51	118.09	19.55	45.7	0.8734
5	0.27	2	30	0.17	129.27	24.81	46.9	0.9853
6	0.27	3	18	0.34	118.82	17.03	44.08	0.8206
7	0.54	1	30	0.34	128.55	21.69	44.9	0.9175
8	0.54	2	18	0.51	108.18	19.31	39.11	0.8001
9	0.54	3	25	0.17	121.45	22.36	43.31	0.9043
*k*1	0.8774	0.8815	0.8247	0.9144				
*k*2	0.8931	0.8849	0.8823	0.8691				
*k*3	0.8740	0.8780	0.9374	0.8609				
Range *R*	0.0191	0.0068	0.1126	0.0534				

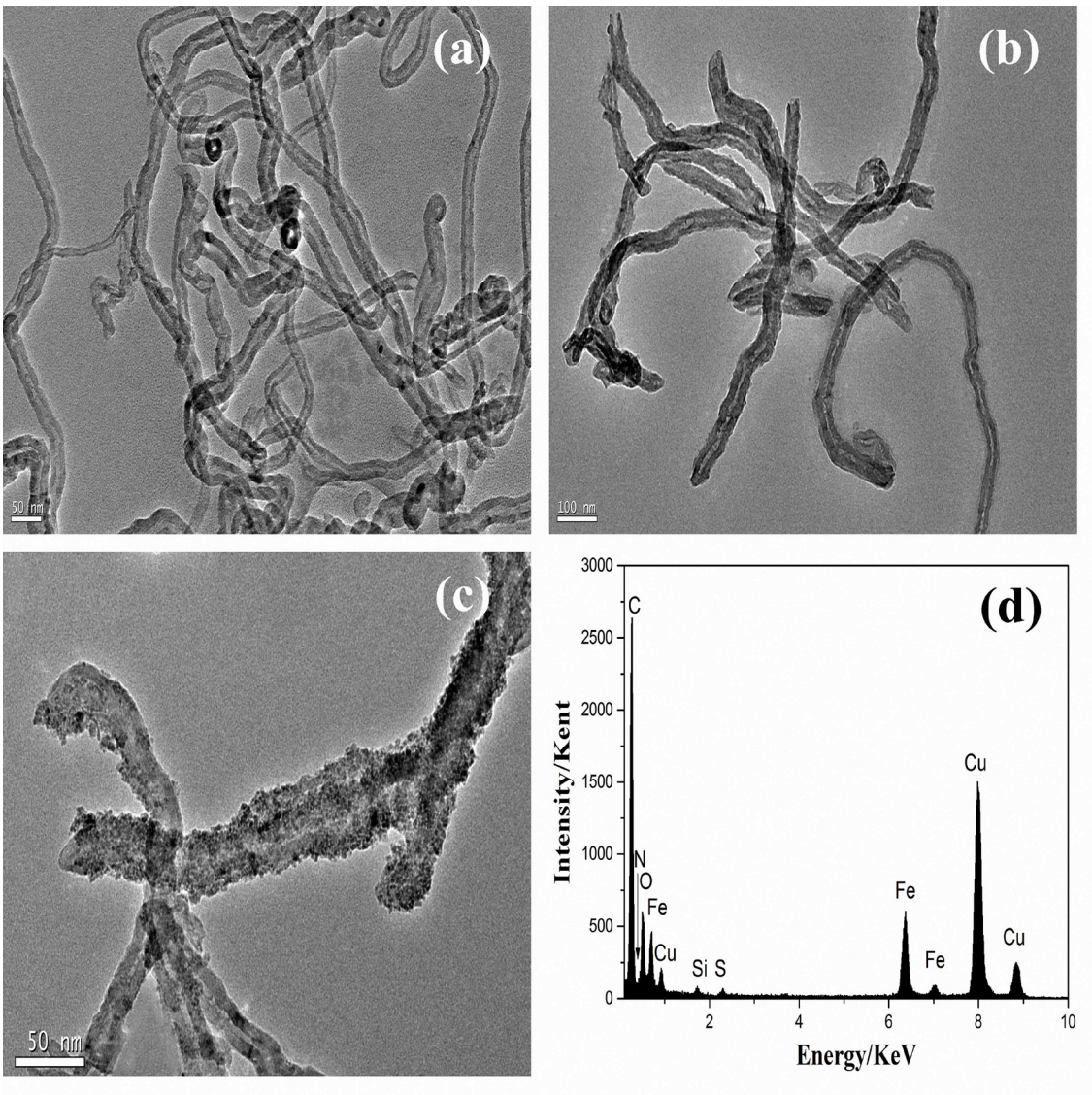

Fig. 3. TEM images of MWCNTs and the composite: (a) original MWCNTs, (b) purified MWCNTs, (c) NH_2-SH-Fe_3O_4/o-MWCNTs, and (d) Energy spectrum of the NH_2-SH-Fe_3O_4/o-MWCNTs.

surface of the CNTs, while the occurrence of the Fe element proved that numerous Fe_3O_4 nanoparticles appeared on the surface of the CNTs, and the Si and S elements were taken from the sulfhydryl groups. The presence of sulfhydryl and amino groups indicated the successful preparation of NH_2-SH-Fe_3O_4/o-MWCNTs.

3.3. FT-IR

Fig. 4 displays FT-IR spectra of purified MWCNTs and NH_2-SH-Fe_3O_4/o-MWCNTs. As shown in Figs. 4(a) and (b), strong stretching absorption peaks at 1,560 cm^{-1} are from C=C stretching in the MWCNTs. This implied that the natural structure of the MWCNTs was not damaged by the group modification. Fig. 4(a) shows a strong absorption peak at 1,107 cm^{-1} caused by C–O [17]. The presence of these oxygen-containing groups provided many adsorption sites to adsorb the metal ions and phenol. However, the C–O vibration peak in the FT-IR spectrum of the NH_2-SH-Fe_3O_4/o-MWCNTs was red shifted compared with the purified MWCNTs because the reaction occurred with the oxygen-containing functional groups on the surface of the CNTs. Fig. 4(a) shows that a new strong peak occurred at 591 cm^{-1}, which corresponded to the stretching vibration of Fe-O [18]. The result verified that Fe_3O_4 nanoparticles were successfully loaded on the surface of the CNTs. Additionally, a new absorption peak appeared at 891 cm^{-1}, which is assigned to stretching of the Si-O bond [19]. The result implied that sulfhydryl was connected to oxygen-containing functional groups on the surface of the CNTs. The result also directly corroborated that sulfhydryl was successfully modified on the surface of the CNTs. The absorption peak at 3,428 cm^{-1} was assigned to stretching of the O–H bond [20]. This proved that hydroxyl was added on the external surface and defected sites of the CNTs after the acid treatment to increase the hydrophilicity and dispersion of NH_2-SH-Fe_3O_4/o-MWCNTs.

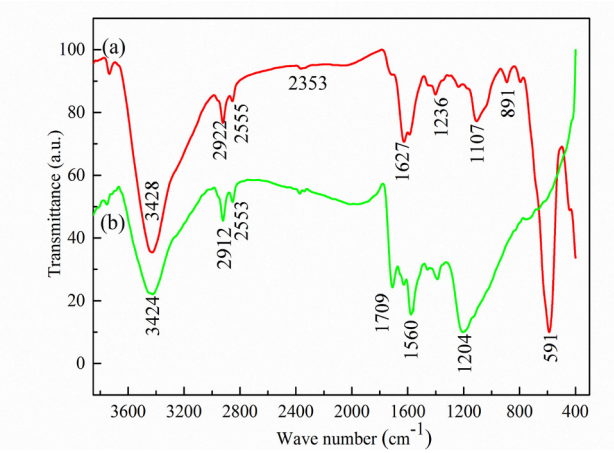

Fig. 4. FT-IR spectra of NH_2-SH-Fe_3O_4/o-MWCNTs: (a) NH_2-SH-Fe_3O_4/o-MWCNTs and (b) purified CNTs.

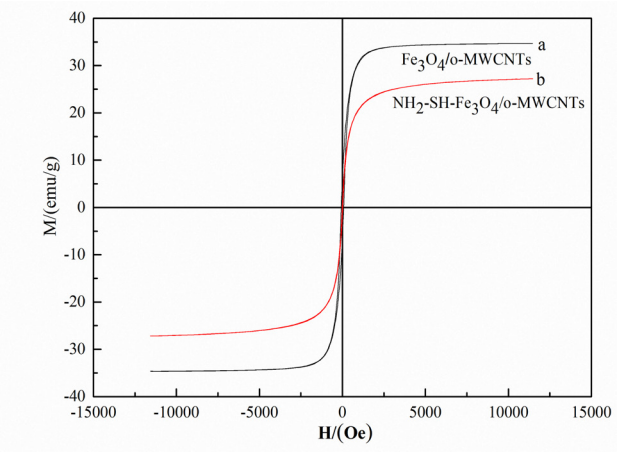

Fig. 5. Hysteresis curves of the Fe_3O_4/MWCNTs (a) and NH_2-SH-Fe_3O_4/MWCNTs (b).

These oxygen-containing functional groups could be connected to polar functional groups (–SH) through hydrogen bonds. Additionally, the interactive effect improved among the groups when the oxygen content on the surface of the NH_2-SH-Fe_3O_4/o-MWCNTs increased. The peak between 1,200 and 1,260 cm^{-1} was caused by stretching of the carboxylic group [21], while that between 2,800 and 3,000 cm^{-1} was less intense than the symmetric and asymmetric $–CH_2$ stretching bands [22]. The reinforced stretching vibration peak of $–CH_2$ came from methylene groups of MPTS [23], which also signified that sulfhydryl groups covered the surface of the oxidized CNTs. The absorption peak at 2,353 cm^{-1} was related to the $–NH_2$ groups while that at 1,627 cm^{-1} belonged to the stretching vibration peak of N–H. The results indicated that the amino group was successfully loaded on the surface of the oxidized CNTs. The above analysis fully revealed that amino and sulfhydryl were successfully loaded onto the surface of the MWCNTs to prepare the NH_2-SH-Fe_3O_4/o-MWCNTs.

3.4. Hysteresis curves

Fig. 5 shows the room-temperature hysteresis curves of the Fe_3O_4/o-MWCNTs and NH_2-SH-Fe_3O_4/o-MWCNTs. The hysteresis curves of the Fe_3O_4/o-MWCNTs and NH_2-SH-Fe_3O_4/MWCNTs both crossed the origin, which indicated that the two materials showed superparamagnetism but no coercivity or remanence [24]. The saturated magnetization intensities of Fe_3O_4/o-MWCNTs and NH_2-SH-Fe_3O_4/MWCNTs were 34.65 and 27.17 emu/g, respectively. The high saturated magnetization intensity indicated that the composite materials could be separated rapidly from an aqueous solution. Because the prepared adsorbents show magnetism, the adsorbents could be isolated from the aqueous solution using a simple magnet. The result showed that the saturated magnetization intensity of the composite materials modified by groups significantly declined. Numerous non-magnetic groups that were modified on the surface of the Fe_3O_4/o-MWCNTs greatly reduced the saturated magnetization intensity of the composite. These results indicated that the prepared magnetic composite materials could be isolated from aqueous solutions, which is favorable for recycling and reutilizing adsorbents to reduce the preparation cost of the adsorbents.

3.5. XPS

XPS is commonly used to analyze the functional groups on the surface of composite materials. Table 3 shows the element types and percentage of atoms in the NH_2-SH-Fe_3O_4/o-MWCNTs. There are six elements (C, Fe, N, O, S, and Si) in the NH_2-SH-Fe_3O_4/o-MWCNTs, and the percentages of the atoms are 57.99%, 8.14%, 1.76%, 26.40%, 2.26%, and 3.46%, respectively. The extremely high oxygen content corroborates that many oxygen-containing groups (such as carboxyl and hydroxyl) are present on the surface of the NH_2-SH-Fe_3O_4/o-MWCNTs. The presence of Fe, N, S, and Si elements also directly showed that Fe_3O_4 nanoparticles, sulfhydryl groups, and amino groups were present on the surface of the CNTs

Fig. 6(a) illustrates that the C1s spectrum of the NH_2-SH-Fe_3O_4/o-MWCNTs can be divided into four Gaussian energy curves, which are located at 284.6, 285.33, 286.52, and 288.80 eV, corresponding to C=C in the CNTs, C–OH in hydroxyl, C=O and –COOH in carboxyl [25]. The occurrence of the Gaussian peak of N1s verified the presence of N–H in the NH_2-SH-Fe_3O_4/o-MWCNTs, as shown in Fig. 6(b) [26]. Fig. 6(c) indicated strong Gaussian peaks at bonding energies of 710.6 and 724.6 eV, which separately corresponded to Fe2p3/2 and Fe2p1/2 in Fe_3O_4. Moreover, the satellite peak did not appear at high bonding energies, which also showed that the nanoparticles in the composite materials were Fe_3O_4 but not Fe_2O_3 [27–28]. The spectrum in Fig. 6(d) contains S–H and C–SH peaks near 163.67 and 164.73 eV, respectively. The presence of these peaks directly verified that the sulfhydryl group was present and was connected to the MWCNTs [29]. The spectrum of Si2p in Fig. 6(e) shows three peaks at bonding energies of 100.8, 102.2, and 102.9 eV. They correspond to C-Si, Si-N, and Si-O groups, respectively [30]. Additionally, the occurrence of Si-N implied that the amino group was connected to sulfhydryl, and the two groups were successfully

loaded onto the surface of the CNTs, which conformed to the results from the infrared analysis [31–32]. Fig. 6(f) shows that there were also six elements appearing in the NH_2-SH-Fe_3O_4/o-MWCNTs.

3.6. Influence of time on the adsorption process and adsorption kinetics

The adsorption kinetics were carried out under a magnetic field intensity of 0.27 *T*, temperature of 30°C, water velocity of 0.12 m/s, and initial concentration of 50 mg/L. Fig. 7 displays the influence of the synergistic effect between the magnetic field and the NH_2-SH-Fe_3O_4/o-MWCNTs on the adsorption capacity for Mg^{2+}, Cd^{2+}, and phenol in the circulating water. The adsorption capacities for Mg^{2+}, Cd^{2+}, and phenol under the synergistic effect between the magnetic field and the NH_2-SH-Fe_3O_4/o-MWCNTs rapidly increased and then stabilized. As shown in Fig. 7, within 60 min, the adsorption capacity of NH_2-SH-Fe_3O_4/o-MWCNTs for Mg^{2+} dramatically increased, reaching 124.27 mg/g at 60 min. Then the adsorption rate significantly decreased with time; the adsorption capacity was generally stable, reaching an equilibrium state (adsorption capacity of 131.64 mg/g) after 8 h. Such a short time for the adsorption equilibrium showed that the prepared adsorbents had a high-efficiency adsorption capacity. The NH_2-SH-Fe_3O_4/o-MWCNTs exhibited a high adsorption rate and promising prospects for industrial applications. The adsorption capacity rapidly grew during the initial adsorption phases because of the large number of exposed areas on the surface of the NH_2-SH-Fe_3O_4/o-MWCNTs. Therefore, Mg^{2+} could randomly occupy the adsorption surface. The adsorptive surface gradually declined with time; therefore, the adsorption rate at the late adsorption phase significantly reduced. Consequently, the surface of the NH_2-SH-Fe_3O_4/o-MWCNTs was completely occupied and reached adsorption saturation. The adsorption reached an equilibrium state after 8 h; therefore, all subsequent experiments were sustained for 8 h.

Fig. 7 indicates that the adsorption capacity for Cd^{2+} significantly increased with time and reached an equilibrium state at 60 min with an equilibrium adsorption

Table 3
Energy, peak area, and element percentage in the NH_2-SH-Fe_3O_4/o-MWCNTs

Name	Binding energy (eV)	Peak area (%)	Element percentage (%)
C1s	284.78	0.57	57.99
Fe2p	711.2	0.08	8.14
N1s	400.42	0.02	1.76
O1s	530.67	0.26	26.4
S2p	163.91	2	2.26
Si2p	102.57	0.03	3.46

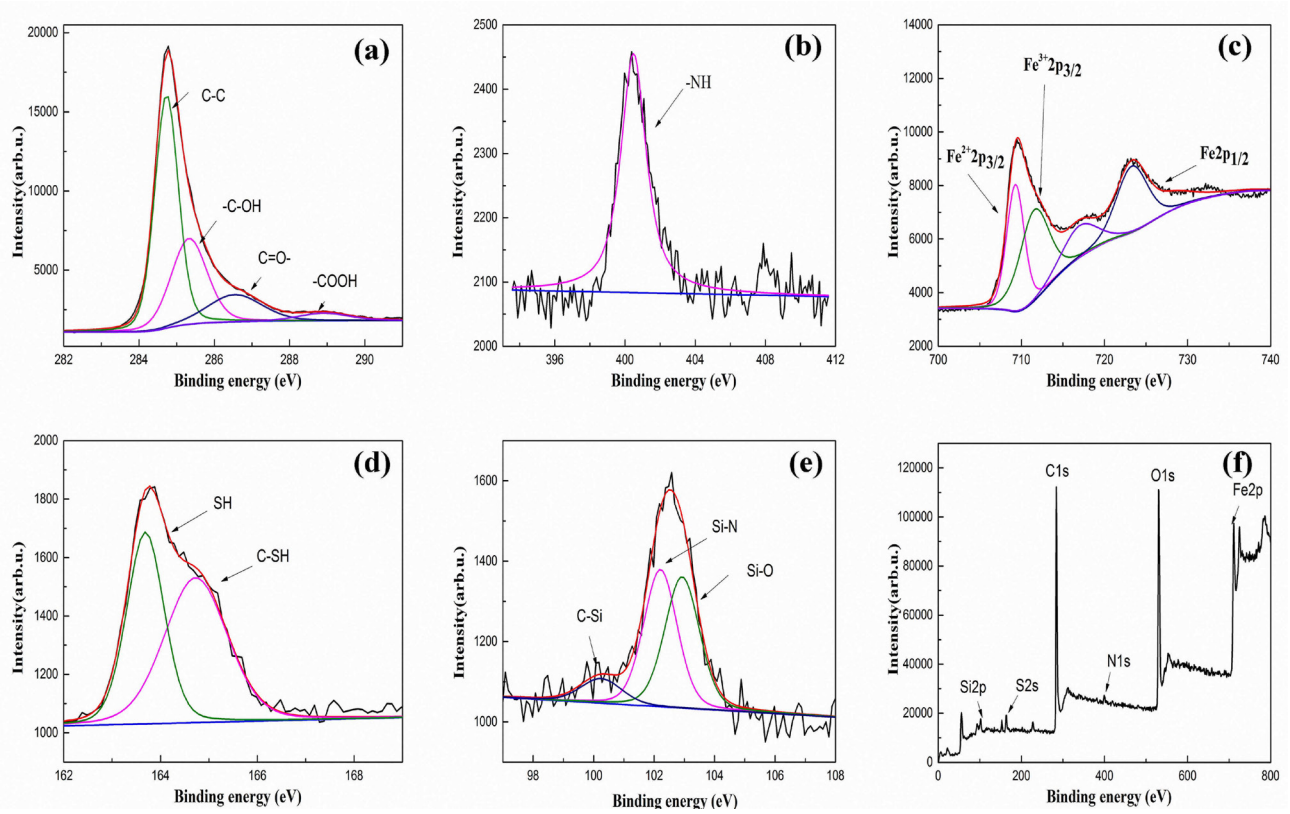

Fig. 6. XPS wide scan spectra of the NH_2-SH-Fe_3O_4/o-MWCNTs: (a) C1s, (b) N1s, (c) Fe2p, (d) S2p, (e) Si2p, and (f) wide scan. The experimental data were fit with Gaussian components assigned to specific chemical bonds, as indicated, and the best fits are plotted in the figures.

capacity of 19.80 mg/g. During the initial adsorption phase, the adsorption rate for Cd^{2+} also rapidly increased but substantially declined at 60 min. The adsorption capacity was generally stable with time. The adsorption capacity of the NH_2-SH-Fe_3O_4/o-MWCNTs for Cd^{2+} was far lower than that for Mg^{2+} because the electronegativity of Mg^{2+} (17.13) was larger than that of Cd^{2+} (9.79). The electronegativity of the ions was highly related to the adsorption and the combination between the metal ions and adsorbents [26]. The adsorption curve for phenol rapidly increased and then stabilized, showing an equilibrium adsorption capacity of 40.15 mg/g.

The adsorption process was fit separately using pseudo-first-order and pseudo-second-order kinetic models. The pseudo-first-order kinetic model can be expressed as follows:

$$\ln\left(q_e - q_t\right) = \ln q_e - k_1 t \tag{2}$$

The pseudo-second-order kinetic model can be calculated as follows:

$$\frac{t}{q_t} = \frac{1}{k_2 q_e^2} + \frac{t}{q_e} \tag{3}$$

where t, q_e, q_t, k_1, and k_2 refer to the time (min), adsorption capacity (mg/g) under an adsorption equilibrium state, adsorption capacity (mg/g) at t, pseudo-first-order adsorption rate constant (mg/g), and pseudo-second-order adsorption rate constant (g/(mg·min)), respectively.

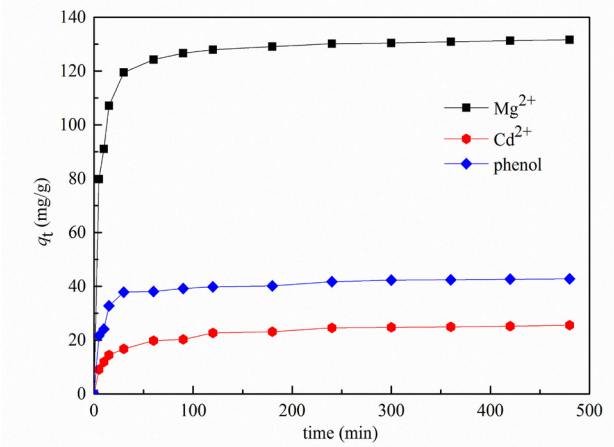

Fig. 7. Effect of time on the adsorption capacities of the NH_2-SH-Fe_3O_4/o-MWCNTs for Mg^{2+}, Cd^{2+}, and phenol (magnetic field intensity of 0.27 T, temperature of 30°C, water velocity of 0.12 m/s, and initial concentration of 50 mg/L).

Table 4 displays the acquired fitting parameters for the equations of the pseudo-first-order and pseudo-second-order kinetic models. Table 4 shows that the adsorption process of the NH_2-SH-Fe_3O_4/o-MWCNTs for Mg^{2+}, Cd^{2+}, and phenol was more consistent with the pseudo-second-order kinetic model than the pseudo-first-order kinetic model and showed a high correlation coefficient. The fitted correlation coefficients of the pseudo-second-order and pseudo-first-order kinetic models of the NH_2-SH-Fe_3O_4/o-MWCNTs for Mg^{2+} were $R^2 = 1$ and $R^2 = 0.908$, respectively. This indicated that the pseudo-second-order kinetic model was more applicable for describing the kinetic adsorption process of the NH_2-SH-Fe_3O_4/o-MWCNTs for Mg^{2+}. Additionally, the adsorption capacity of the NH_2-SH-Fe_3O_4/o-MWCNTs for Mg^{2+} was 131.58 mg/g, which was obtained based on the pseudo-second-order kinetic model and was closer to the experimental data ($q_{e,exp}$ = 131.64 mg/g) than that based on the pseudo-first-order kinetic model. When fitting the kinetic data of adsorbed phenol, the same phenomenon could be observed, which implied that the pseudo-second-order kinetic model could more favorably describe the kinetic process of the NH_2-SH-Fe_3O_4/o-MWCNTs for Mg^{2+}, Cd^{2+}, and phenol. Namely, the adsorption rate was controlled by the chemical adsorption mechanism. Additionally, the pseudo-second-order adsorption rates for adsorbing Mg^{2+}, Cd^{2+}, and phenol were 2×10^{-3}, 2.3×10^{-3}, and 3×10^{-3} g/(mg·min), respectively. These similar values indicated that the adsorption rates of the adsorbents for Mg^{2+}, Cd^{2+}, and phenol were nearly the same.

3.7. Isotherm adsorption

The isotherm adsorption is typically used to analyze the adsorption data and explore the adsorption mechanism. The Langmuir and Freundlich isotherm models are two common models to investigate the adsorption mechanism. The Langmuir model is mainly used to describe uniform and monolayer adsorptions, which assume that all adsorption sites on the surface of the adsorbents exhibit the same attractive force toward the adsorbates [20]. If the adsorption process conforms to the Langmuir isotherm model, the maximum adsorption capacity of the adsorbent can be inferred from the fitting results. In contrast, the Freundlich isotherm model assumes that the adsorption process is non-uniform with multi-layer adsorption. The Langmuir isotherm model can be expressed as follows:

$$\frac{C_e}{q_e} = \frac{1}{K_L q_m} + \frac{C_e}{q_m} \tag{4}$$

Table 4
Parameters of pseudo-first-order and pseudo-second-order kinetic models

Adsorbate	Pseudo-first order			Pseudo-second order		
	q_{ca} (mg/g)	k_1(1/min)	R^2	q_{ca}(mg/g)	K_2 (g/mg/min)	R^2
Mg^{2+}	131.64	0.0105	0.908	131.58	0.002	1
Cd^{2+}	25.53	0.0088	0.969	26.11	0.0023	0.992
Phenol	42.72	0.011	0.951	43.29	0.003	0.998

where C_e, q_e, and q_m represent the concentration (mg/L) of the solution, equilibrium adsorption capacity (mg/g) of the adsorbents under the adsorption equilibrium state, and maximum adsorption capacity (mg/g), respectively. C_e is determined by plotting C_e/q_e against C_e. The adsorption constant, K_L, and q_m can be obtained from the slope and intercept of a straight line, respectively. The Freundlich isotherm model assumes that the adsorption process occurs on the surface of a non-uniform medium. Different adsorption sites show different bonding energies and affinities, and the adsorption process is a multi-layer adsorption. The Freundlich isotherm model can be expressed as follows:

$$\ln q_e = \ln k_f + \frac{1}{n}\ln C_e \tag{5}$$

where q_e and C_e refer to the adsorption capacity (mg/g) of the adsorbent and concentration (mg/L) of the target pollutant under an adsorption equilibrium state, respectively. Moreover, k_f and n represent the constants separately related to the adsorption capacity and adsorption intensity, respectively. The adsorption data were fit by employing the Langmuir and Freundlich isotherm models according to Eqs. (4) and (5). The fitting results are displayed in Fig. 8, and the fitting parameters are shown in Table 5. As shown by the correlation coefficient (R^2) in Table 5, the adsorption process of the NH_2-SH-Fe_3O_4/o-MWCNTs for Mg^{2+} and Cd^{2+} was more consistent with the Langmuir isotherm model. By taking the adsorption process for Mg^{2+} as an example, the correlation coefficients of the Langmuir and Freundlich models were 0.988 and 0.974, respectively. As shown by the correlation coefficient (R^2) in Table 5, the adsorption process of the NH_2-SH-Fe_3O_4/o-MWCNTs for Mg^{2+} and Cd^{2+} was consistent with the Langmuir isotherm model, which implies that Mg^{2+} and Cd^{2+} did not self-interact and is consistent with monolayer adsorption. According to the calculation formula for the Langmuir isotherm model, the maximum adsorption capacities, q_m, of the NH_2-SH-Fe_3O_4/o-MWCNTs for Mg^{2+} and Cd^{2+} were 161.29 and 39.06 mg/g, respectively. Based on the value of R^2, the adsorption process of the NH_2-SH-Fe_3O_4/o-MWCNTs for phenol was more consistent with the Freundlich isotherm model than the Langmuir isotherm model. Therefore, phenols were adsorbed on the surface of adsorbents and there were interactive effects among the phenols because the adsorption capacity of the adsorbents for phenol was larger than that for Cd^{2+}. The results indicate that the prepared NH_2-SH-Fe_3O_4/o-MWCNTs are high-efficiency adsorbents with industrial applications.

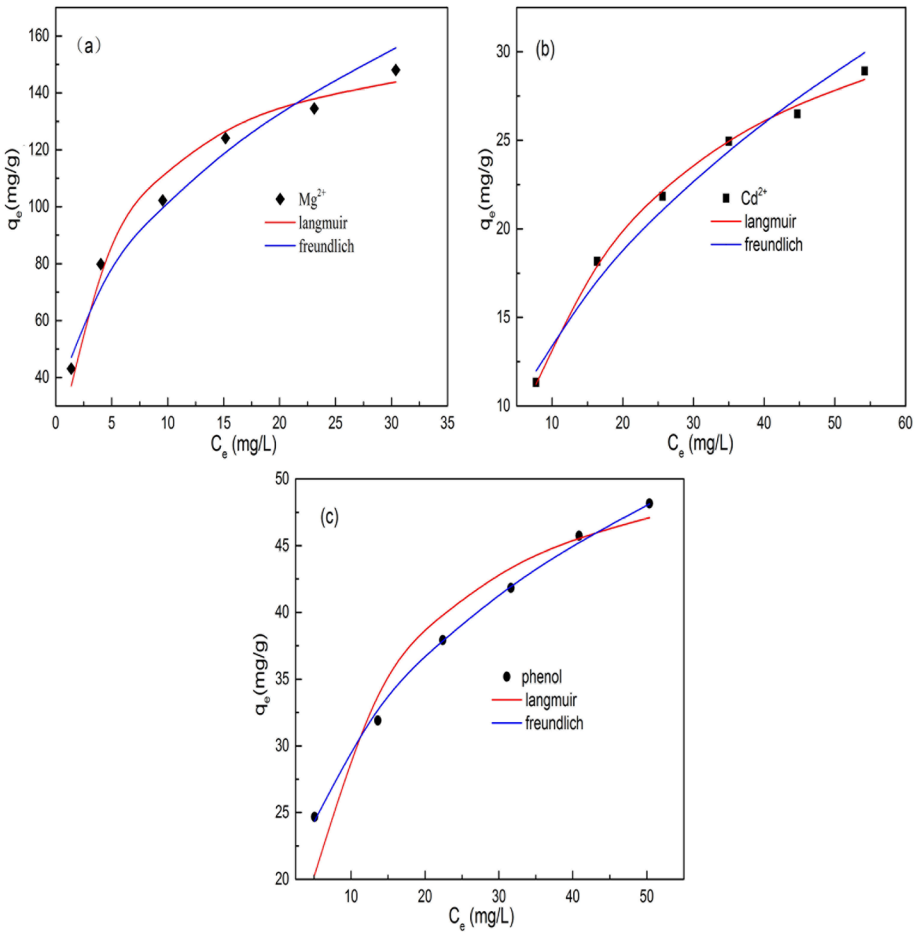

Fig. 8. The Langmuir and Freundlich isotherm models for (a) Mg^{2+}, (b) Cd^{2+} and (c) phenol.

Table 5
Parameters of Langmuir and Freundlich model

Model	Parameters	Mg^{2+}	Cd^{2+}	Phenol
Langmuir	q_m (mg g^{-1})	161.29	39.06	55.249
	K_L	0.208	0.0527	0.112
	R^2	0.988	0.998	0.991
Freundlich	K_f	41.59	4.574	15.062
	N	2.5853	2.1245	3.374
	R^2	0.974	0.981	0.997

Table 6
Thermodynamic parameters of the adsorption processes for Mg^{2+}, Cd^{2+}, and phenol

	T/°C	lnK_d	$\Delta G°$ (kJ/mol)	$\Delta H°$ (kJ/mol)	$\Delta S°$ (J/(mol·K))
Mg^{2+}	18	10.089	–34.635	10.25	119.056
	25	10.170	–35.469		
	30	10.259	–36.064		
Cd^{2+}	18	8.220	–22.413	2.537	77.029
	25	8.232	–22.952		
	30	8.264	–23.337		
Phenol	18	9.199	–25.661	3.415	88.195
	25	9.226	–26.279		
	30	9.256	–26.72		

3.8. Influence of temperature on the thermodynamics

The adsorption process of NH_2-SH-Fe_3O_4/o-MWCNTs for Mg^{2+}, Cd^{2+}, and phenol is a spontaneous adsorption with a large adsorption driving force. As the temperature increased, the Gibbs free energy gradually declined, implying that the adsorption process was effective at a high temperature. Increasing the temperature improves the adsorption process. The NH_2-SH-Fe_3O_4/o-MWCNTs adsorbed a higher amount of Mg^{2+} than Cd^{2+} and phenol. Additionally, the physical, physicochemical, and chemical adsorption processes generally appeared from –20 to 0, –20 to –80, and –80 to –400 kJ/mol, respectively [33–35]. Therefore, the type of adsorption process of the NH_2-SH-Fe_3O_4/o-MWCNTs for Mg^{2+}, Cd^{2+}, and phenol could be determined from the calculated Gibbs free energy. Table 6 shows that the adsorption process of the NH_2-SH-Fe_3O_4/o-MWCNTs for Mg^{2+}, Cd^{2+}, and phenol occurred under the synergistic effect between the physical and chemical adsorptions. The functional groups (such as sulfhydryl and amino) on the surface of the NH_2-SH-Fe_3O_4/o-MWCNTs formed chemical bonds with Mg^{2+} and Cd^{2+} in solution to improve the adsorption capacity. Additionally, phenol adsorption depended on the polar groups on the surface of the adsorbents. When a limited number of polar groups were present, the adsorption capacity for phenols was low. The positive enthalpy change indicated that the adsorption process was endothermic, and increasing the temperature promoted the adsorption of Mg^{2+}, Cd^{2+}, and phenols. Therefore, moderately increasing the temperature favored the adsorption of Mg^{2+}, Cd^{2+}, and phenols. A high entropy change indicated a significant entropy process during the adsorption and that the solid-liquid interface was subjected to a chaotic state. The entropy change was likely caused by the presence of water molecules during the ion exchange reaction, the good affinity of NH_2-SH-Fe_3O_4/o-MWCNTs with Mg^{2+}, Cd^{2+}, and phenols, and the increasing randomness of the solution interface during the adsorption process. According to the data in Table 6, the free energy changes were determined, and the specific Eqs. (6)–(8) is displayed as follows:

The adsorption reaction for Mg^{2+}:

$$\Delta G° = 10250 - 119.056T, \quad \text{J/mol} \tag{6}$$

The adsorption reaction for Cd^{2+}:

$$\Delta G° = 2537 - 77.029T, \quad \text{J/mol} \tag{7}$$

The adsorption reaction for phenol:

$$\Delta G° = 3415 - 88.195T, \quad \text{J/mol} \tag{8}$$

Table 7 shows the heats of adsorption from various forces. According to the thermodynamic data, it can be inferred that hydrogen bonds and dipole force are for Mg^{2+}, van der Waals force and hydrogen bonds for Cd^{2+} as well as hydrogen bonds and dipole force for phenol.

3.9. Effect of magnetic field intensity on the adsorption capacities

Fig. 9 displays the influence of the magnetic field intensity on the adsorption capacity of the NH_2-SH-Fe_3O_4/o-MWCNTs. When the magnetic field intensity was 0 T, the equilibrium adsorption capacity of the adsorbent for Mg^{2+} was 104.91 mg/g. When imposing a magnetic field intensity of 0.27 T, the adsorption capacity for Mg^{2+} increased to 109.27 mg/g. The adsorption capacity of the NH_2-SH-Fe_3O_4/o-MWCNTs for Mg^{2+} was 126.09 mg/g when the magnetic field intensity was 0.7 T, increasing by 20.19%. Therefore, the magnetic field promoted the adsorption process for Mg^{2+}. Higher magnetic field intensities provided higher adsorption capacities for Mg^{2+}. The adsorption process for Cd^{2+} exhibited a similar phenomenon. The equilibrium adsorption capacity of the NH_2-SH-Fe_3O_4/o-MWCNTs for Cd^{2+} reached 16.58 mg/g without a magnetic field. The equilibrium adsorption capacity of the NH_2-SH-Fe_3O_4/o-MWCNTs for Cd^{2+} slightly increased as the magnetic field intensity increased. At a magnetic field intensity of 0.54 T, the adsorption capacity reached 27.63 mg/g, which is 66.63% greater than that for the circulating water without a magnetic field. Therefore, the magnetic field can promote the adsorption of the adsorbents for Mg^{2+} and Cd^{2+} under the synergistic effect between the magnetic field and NH_2-SH-Fe_3O_4/o-MWCNTs. However, a different adsorption phenomenon was observed for the phenols.

Fig. 9 shows the adsorption capacity of the adsorbents for phenol gradually declined as the magnetic field intensity increased. When the magnetic field intensity was 0 T,

Table 7
Heats of adsorption from various forces (kJ/mol)

Hydrophobic bond	4
Van der Waals force	1–2
Hydrogen bond	2–40
Inter-polar force	2–29
Chemical bond	>60

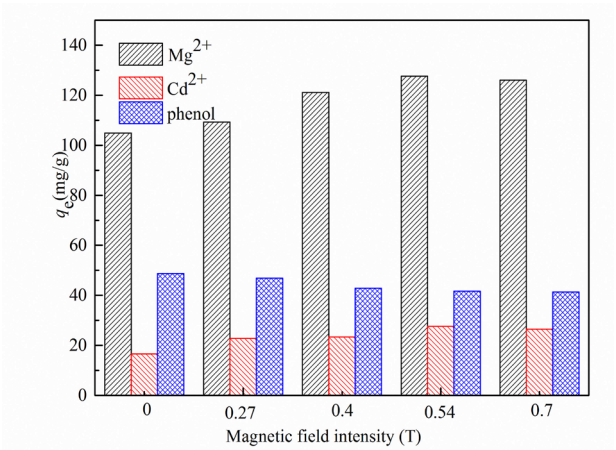

Fig. 9. Effect of the magnetic field intensity on the adsorption capacities of the NH_2-SH-Fe_3O_4/o-MWCNTs for Mg^{2+}, Cd^{2+}, and phenol.

the adsorption capacity for phenol was 48.72 mg/g, and it decreased to 46.90 mg/g when the magnetic field intensity was 0.27 *T*. As the magnetic field intensity increased, the equilibrium adsorption capacity for phenol gradually declined, especially at a magnetic field intensity of 0.27 *T*. The equilibrium adsorption capacity for phenol decreased to 41.31 mg/g when the magnetic field intensity was 0.7 *T*. The magnetic field inhibited the adsorption of the adsorbents for phenol under the synergistic effect between the magnetic field and the NH_2-SH-Fe_3O_4/o-MWCNTs. After the circulating water was subjected to the magnetic treatment, the associative structure of the water molecules changed and the polarity of the water molecules strengthened so that the number of hydrogen bonds increased among the water molecules [36]. During the adsorption process, there were numerous acid oxygen-containing functional groups on the surface of the adsorbent; thus, the adsorbent had a high adsorption capacity for polar materials [37]. Because the polarity of water was larger than that of phenol, the water molecules with a strong polarity could occupy the adsorption sites on the surface of the adsorbents to further decrease the adsorption capacity of the adsorbent for phenols. However, under the effect of the external magnetic field, the charged ions (Mg^{2+} and Cd^{2+}) underwent a cyclotron motion, which was affected by the Lorentz force. Moreover, anions and cations moved in opposite directions, which increased the collision probability between the metal ions and reduced the parcel phenomenon of the water molecular cluster in the outer sphere of metal ions. Therefore, the contact probability between the adsorbent and metal ions rose and increased the adsorption capacity of the adsorbent for Mg^{2+} and Cd^{2+} [38]. Therefore, magnetic field promoted the adsorption of metal ions while it inhibited the adsorption of organics under the synergistic effect between the magnetic field and NH_2-SH-Fe_3O_4/o-MWCNTs.

4. Conclusion

NH_2-SH-Fe_3O_4/o-MWCNT composite was successfully prepared and characterized using TEM, FT-IR, hysteresis curves, and XPS. We investigated the influence of the adsorption performance for Mg^{2+}, Cd^{2+}, and phenols in circulating water under the synergistic effect between the NH_2-SH-Fe_3O_4/o-MWCNTs and a magnetic field. The adsorption process was subjected to thermodynamic analyses. The optimal experimental conditions were a temperature of 30°C, magnetic field intensity of 0.27 *T*, and water velocity of 0.17 m/s. TEM image indicated that Fe_3O_4 nanoparticles with 6 nm of diameter were successfully loaded onto the surface of CNTs. The NH_2-SH-Fe_3O_4/o-MWCNTs exhibited superparamagnetism, but no coercivity or remanence. The adsorption capacities of the adsorbent for Mg^{2+}, Cd^{2+}, and phenol were 124.27, 19.80, and 40.15 mg/g at 60 min respectively. The adsorption processes for Mg^{2+}, Cd^{2+}, and phenol conformed to a pseudo-second-order kinetic model. Additionally, the adsorption processes for Mg^{2+} and Cd^{2+} were consistent with the Langmuir isotherm model, while that for phenol was consistent with Freundlich model. Under the synergistic effect between the magnetic field and NH_2-SH-Fe_3O_4/o-MWCNTs, the magnetic field promoted the adsorption of Mg^{2+} and Cd^{2+} and inhibited the adsorption process for phenol. The application of NH_2-SH-Fe_3O_4/o-MWCNT and magnetic field has a good prospect in water treatment.

Acknowledgments

The authors are grateful for financial support from the National Natural Science Foundation of China (51304101, 51764039), Doctor research cost of Lanzhou university of technology (061702).

References

[1] M.H. Dehghani, M. Mostofi, M. Alimohammadi, G. McKay, K. Yetilmezsoy, A.B. Albadarin, B. Heibati, M. AlGhouti, N.M. Mubarak, J.N. Sahu, High-performance removal of toxic phenol by single-walled and multi-walled carbon nanotubes: kinetics, adsorption, mechanism and optimization studies, J. Ind. Eng. Chem., 35 (2016) 63–74.
[2] J.S. Baker, S.J. Judd, Magnetic amelioration of scale formation, Water. Res., 30 (1996) 247–260.
[3] X. Zhang, G. Liu, D. Cang, C. Song, T. Sun, Mechanism of high-gradient magnetic treatment of circulating cooling water, Iron. Steel., 41 (2006) 82–84.
[4] M. Gryta, The influence of magnetic water treatment on $CaCO_3$ scale formation in membrane distillation process, Sep. Purif. Technol., 80 (2011) 293–299.
[5] M.W. Yap, N.M. Mubarak, J.N. Sahu, E.C. Abdullah, Microwave induced synthesis of magnetic biochar from agricultural biomass for removal of lead and cadmium from wastewater, J. Ind. Eng. Chem., 45 (2017) 287–295.
[6] N.M. Mubarak, J.N. Sahu, E.C. Abdullah, N.S. Jayakumar, Rapid adsorption of toxic Pb(II) ions from aqueous solution using multiwall carbon nanotubes synthesized by microwave chemical vapor deposition technique, J. Environ. Sci., 45 (2016) 143–155.

[7] N.M. Mubarak, R.F. Alicia, E.C. Abdullah, J.N. Sahu, A.B.A. Haslija, J. Tan, Statistical optimization and kinetic studies on removal of Zn^{2+} using functionalized carbon nanotubes and magnetic biochar, J. Environ. Chem. Eng., 1 (2013) 486–495.
[8] N.M. Mubarak, R.K. Thines, N.R. Sajuni, E.C. Abdullah, J.N. Sahu, P. Ganesan, N.S. Jayakumar, Adsorption of chromium (VI) on functionalized and non-functionalized carbon nanotubes, Korean. J. Chem. Eng., 31 (2014) 1582–1591.
[9] N.M. Mubarak, J.N. Sahu, E.C. Abdullah, N.S. Jayakumar, Removal of heavy metals from wastewater, Sep. Purif. Rev., 43 (2014) 311–338.
[10] Y.H. Chen, Z.H. Huang, M.M. Lu, W.Q. Cao, J. Yuan, D.Q. Zhang, M.S. Cao, 3D Fe_3O_4 nanocrystals decorating carbon nanotubes to tune electromagnetic properties and enhance microwave absorption capacity, J. Mater. Chem. A., 3 (2015) 12621–12625.
[11] M. Ruthiraan, N.M. Mubarak, R.K. Thines, E.C. Abdullah, J.N. Sahu, N.S. Jayakumar, P. Ganesan, Comparative kinetic study of functionalized carbon nanotubes and magnetic biochar for removal of Cd^{2+} ions from wastewater, Korean. J. Chem. Eng., 32 (2015) 446–457.
[12] K.A. Mahmoud, B. Mansoor, A. Mansour, M. Khraisheh, Functional graphene nanosheets: the next generation membranes for water desalination, Desalination, 356 (2015) 208–225.
[13] N.M. Bandaru, N. Reta, H. Dalal, A.V. Ellis, J. Shapter, N.H. Voelcker, Enhanced adsorption of mercury ions on thiol derivatized single wall carbon nanotubes, J. Hazard. Mater., 261 (2013) 534–541.
[14] X. Zhang, Q. Huang, M. Liu, J. Tian, G. Zeng, Z. Li, K. Wang, Q. Zhang, Q. Wan, F. Deng, Preparation of amine functionalized carbon nanotubes via a bioinspired strategy and their application in Cu^{2+} removal, Appl. Surf. Sci., 343 (2015) 19–27.
[15] Y. Liu, L. Gao, A study of the electrical properties of carbon nanotube-$NiFe_2O_4$ composites: effect of the surface treatment of the carbon nanotubes, Carbon, 43 (2005) 47–52.
[16] Y.J. Kim, T.S. Shin, H. D. Choi, J.H. Kwon, Y.C. Chung, H.G. Yoon, Electrical conductivity of chemically modified multiwalled carbon nanotube/epoxy composites, Carbon, 43 (2005) 23–30.
[17] J. Maxwell, J. Volpe, C. Barlow, W. Caughey, Infrared evidence for the mode of binding of oxygen to iron of myoglobin from heart muscle, Biochem. Biophys. Res. Commun., 58 (1974) 166–171.
[18] Y.W. Jun, Y.M. Huh, J.S. Choi, J.H. Lee, H.T. Song, S. Kim, S. Yoon, K.S. Kim, J.S. Shin, Nanoscale size effect of magnetic nanocrystals and their utilization for cancer diagnosis via magnetic resonance imaging, J. Am. Chem. Soc., 127 (2005) 5732–5733.
[19] H. Wang, J. Fang, T. Cheng, J. Ding, L. Qu, L. Dai, X. Wang, T. Lin, One-step coating of fluoro-containing silica nanoparticles for universal generation of surface superhydrophobicity, Chem. Commun., 7 (2008) 877–879.
[20] R.K. Thines, N.M. Mubarak, M. Ruthiraan, E.C. Abdullah, J.N. Sahu, N.S. Jayakumara, P. Ganesan, N.R. Sajuni, Adsorption isotherm and thermodynamics studies of Zn(II) on functionalized and non-functionalized carbon nanotubes, Adv. Sci., 6 (2014) 1–11.
[21] C. Zhang, J. Sui, J. Li, Y. Tang, W. Cai, Efficient removal of heavy metal ions by thiol-functionalized superparamagnetic carbon nanotubes, Chem. Eng. J., 210 (2012) 45–52.
[22] L. Kong, X. Yin, X. Yuan, Y. Zhang, X. Liu, L. Cheng, L. Zhang, Electromagnetic wave absorption properties of graphene modified with carbon nanotube/poly (dimethyl siloxane) composites, Carbon, 73 (2014) 185–193.
[23] Y.M. Huh, Y.W. Jun, H.T. Song, S. Kim, J.S. Choi, J.H. Lee, S. Yoon, K.S. Kim, J.S. Shin, J.S. Suh, In vivo magnetic resonance detection of cancer by using multifunctional magnetic nanocrystals, J. Am. Chem. Soc., 127 (2005) 12387–12391.
[24] R. Singh, R. Verma, G. Sumana, A.K. Srivastava, S. Sood, R.K. Gupta, B. Malhotra, Nanobiocomposite platform based on polyaniline-iron oxide-carbon nanotubes for bacterial detection, Bioelectrochemistry., 86 (2012) 30–37.
[25] N.M. Mubarak, J.N. Sahu, E.C. Abdullah, N.S. Jayakumar, P. Ganesan, Microwave assisted multiwall carbon nanotubes enhancing Cd(II) adsorption capacity in aqueous media, J. Ind. Eng. Chem., 24 (2015) 24–33.
[26] N.M. Mubarak, J.N. Sahu, E.C. Abdullah, N.S. Jayakumar, P. Ganesan, Novel microwave-assisted multiwall carbon nanotubes enhancing Cu (II) adsorption capacity in water, J. Taiwan Inst. Chem. E., 53 (2015) 140–152.
[27] N.M. Mubarak, J.N. Sahu, E.C. Abdullah, N.S. Jayakumar, P. Ganesan, Microwave-assisted synthesis of multi-walled carbon nanotubes for enhanced removal of Zn(II) from wastewater, Res. Chem. Intermed., 42 (2016) 3257–3281.
[28] M. Ruthiraan, N.M. Mubarak, R.K. Thines, E.C. Abdullah, J.N. Sahu, N.S. Jayakumar, P. Ganesan, Comparative kinetic study of functionalized carbon nanotubes and magnetic biochar for removal of Cd^{2+} ions from wastewater, Korean. J. Chem. Eng., 32 (2015) 446–457.
[29] F. Sinapi, J. Delhalle, Z. Mekhalif, XPS and electrochemical evaluation of two-dimensional organic films obtained by chemical modification of self-assembled monolayers of (3-mercaptopropyl) trimethoxysilane on copper surfaces, Mat. Sci. Eng., 22 (2002) 345–353.
[30] W. Li, B. Zhou, M. Wang, Z. Li, R. Ren, Silane functionalization of graphene oxide and its use as a reinforcement in bismaleimide composites, J. Mater. Sci., 50 (2015) 5402–5410.
[31] X. Song, Y. Zhang, C. Yan, W. Jiang, C. Chang, The Langmuir monolayer adsorption model of organic matter into effective pores in activated carbon, J. Colloid. Interface. Sci., 389 (2013) 213–219.
[32] J. Perić, M. Trgo, N.V. Medvidović, Removal of zinc, copper and lead by natural zeolite-a comparison of adsorption isotherms, Water. Res., 38 (2004) 1893–1899.
[33] N.M. Mubarak, J.N. Sahu, E.C. Abdullah, N.S. Jayakumar, P. Ganesan, Single stage production of carbon nanotubes using microwave technology, Diamond. Relat. Mater., 48 (2014) 52–59.
[34] L.L. Jiang, S.J. Li, H.T. Yu, Z.S. Zou, X.G. Hou, F.M. Shen, C.T. Li, X.Y. Yao, Amino and thiol modified magnetic multi-walled carbon nanotubes for the simultaneous removal of lead, zinc, and phenol from aqueous solutions, Appl. Surf. Sci., 369 (2016) 398–413.
[35] A.M. Carmo, L.S. Hundal, M.L. Thompson, Sorption of hydrophobic organic compounds by soil materials: application of unit equivalent Freundlich coefficients, Environ. Sci. Technol., 34 (2000) 4363–4369.
[36] R. Cai, H. Yang, J. He, W. Zhu, The effects of magnetic fields on water molecular hydrogen bonds, J. Mol. Struct., 938 (2009) 15–19.
[37] V. Datsyuk, M. Kalyva, K. Papagelis, J. Parthenios, D. Tasis, A. Siokou, I. Kallitsis, C. Galiotis, Chemical oxidation of multi-walled carbon nanotubes, Carbon, 46 (2008) 833–840.
[38] B. Song, P. Xu, G.M. Zeng, J.L. Gong, X.X. Wang, J. Yan, S.F. Wang, P. Zhang, W.C. Cao, S.J. Ye, Modeling the transport of sodium dodecyl benzene sulfonate inriverine sediment in the presence of multi-walled carbon nanotubes, Water. Res., 129 (2018) 20–28.